

Robust Iris Segmentation under Unconstrained Settings

João C. Monteiro, Hélder P. Oliveira, Ana F. Sequeira and Jaime S. Cardoso

INESC TEC (formerly INESC Porto) and Faculdade de Engenharia, Universidade do Porto, Porto, Portugal

Keywords: Biometrics, Iris Segmentation, Unconstrained Environment, Gradient Flow, Shortest Closed Path.

Abstract: The rising challenges in the field of iris recognition, concerning the development of accurate recognition algorithms using images acquired under an unconstrained set of conditions, is leading to a renewed interest in the area. Although several works already report excellent recognition rates, these values are obtained by acquiring images in very controlled environments. The use of such systems in daily security activities, such as airport security and bank account management, is therefore hindered by the inherent unconstrained nature under which images are to be acquired. The proposed work focused on mutual context information from iris centre and iris limbic contour to perform robust and accurate iris segmentation in noisy images. A random subset of the UBIRIS.v2 database was tested with a promising E^1 classification rate of 0.0109.

1 INTRODUCTION

In almost everyone's daily activities, personal identification plays an important role. The most traditional techniques to achieve this goal are knowledge-based and token-based automatic personal identifications. Token-based approaches take advantage of a personal item, such as a passport, driver's license, ID card, credit card or a simple set of keys to distinguish between individuals. Knowledge-based approaches, on the other hand, are based on something the user knows that, theoretically, nobody else has access to, for example passwords or personal identification numbers. Both of these approaches present obvious disadvantages: tokens may be lost, stolen, forgotten or misplaced, while passwords can easily be forgotten by a valid user or guessed by an unauthorized one (Jain et al., 2000). In fact, all of these approaches stumble upon an obvious problem: any piece of material or knowledge can be fraudulently acquired.

Biometrics represents a return to a more natural way of identification. Testing someone by what this someone is, instead of relying on something he owns or knows seems likely to be the way forward.

Several biological traits in humans show a considerable inter-individual variability: fingerprints and palmprints, the shape of the ears, the pattern of the iris, among others. Biometrics works by recognizing patterns within these biological traits, unique to each individual, to increase the reliability of recognition. The growing need for reliability and robustness,

raised some expectations and became the focal point of attention for research works on biometrics. The choice of a specific biometric trait is weighted by a set of qualitative values that describe its overall quality: universality, uniqueness, collectability and permanence (Jain et al., 2000). With all these variables in mind, the iris presents itself as a leading candidate to become the standard biometric trait: it is universal, the variability is huge which assures the uniqueness for each individual, apart from being an organ easily accessible and very difficult to modify.

Even though excellent rates of recognition are found in literature (Daugman, 2006), these results are associated with a set of acquisition conditions that constrain the quality of the tested images. The majority of the developed iris recognition systems rely on near-infrared (NIR) imaging rather than visible light (VL). This is due to the fact that fewer reflections from the cornea in NIR imaging result in maximized signal-to-noise ratio (SNR) in the sensor, thus improving the contrast of iris images and the robustness of the system. NIR imaging, however, presents a series of hazards, as no instinctive response (such as blinking) is triggered in response to excessively strong illumination. Another typically imposed constraint to the user of an iris recognition system is the need to stop-and-stare at a close distance to the sensor (i.e. user collaboration). These factors create important limitations to the applicability of iris recognition algorithms in real-life conditions, such as military applications or bank account management. The develop-

ment of iris recognition algorithms that are capable of encompassing such limitations has been gaining focus in recent years.

In this work we focus on *iris segmentation*, as proposed in (Daugman, 1993). Iris segmentation consists on the detection of the two defining contours of the iris region. In the eye region, three main regions can be easily distinguished: the *sclera*, also known as the white of the eye, is the most easily distinguishable part of the eye, surrounding the *iris*, the coloured region of the eye; inside the iris, a darker region is distinguishable, corresponding to the *pupil*, the region through which light enters the eye. Besides its distinctive properties as a biometric trait, the iris is also a contractile structure responsible to adapt the size of the pupil, so as to regulate the amount of light that enters the eye. Two main contours can be defined as the separating boundaries of the three aforementioned regions: the *limbic contour* separates the iris from the sclera, and the *pupillary contour*, the iris from the pupil. The detection of these contours is the main goal of segmentation and an essential step in the development of high accuracy recognition systems.

We argue that iris segmentation can benefit from the simultaneous detection of the iris centre and iris external contour. When performed independently, both tasks are nontrivial since many other parts of the image may be falsely detected. However, the two tasks can benefit greatly from serving as context for each other. Central to our method to detect iris centre candidates is the use of gradient flow information with a specific gradient vector field template; the detection of the limbic contour relies on the search of strong closed contours around the centre candidates.

The remainder of this paper is organized as follows: Section 2 summarizes relevant works concerning iris segmentation; Section 3 includes an algorithm overview; the theoretical basis behind the developed algorithm; a detailed analysis of the different steps of the limbic contour segmentation algorithm; Section 4 presents the obtained results and finally the conclusions and future prospects are summarized in Section 5.

2 RELATED WORK

The original approach to the segmentation task was proposed by Daugman (Daugman, 1993) and consisted in the maximisation of an integro-differential operator. In a different approach, Wildes (Wildes, 1997) suggested a method involving edge detection followed by circular Hough transform (CHT). For years, several works in the iris biometrics field fo-

cused on Daugman's and Wilde's algorithms, presenting variations at many levels.

One example is the CHT-based method used for the segmentation step in Masek's algorithm (Masek, 2003). Ma et al. (Ma et al., 2004) created a system that mixed both the CHT segmentation approach and the rubber sheet model normalization, introducing some concepts like pre-processing of iris images for specular reflection removal.

The integro-differential operator and the CHT are still widely used for segmenting iris images, offering good segmentation accuracy but also computational complexity. Radman et al. (Radman et al., 2012) addresses a simple solution for this problem by localizing the initial center of the pupil using a circular Gabor filter (CGF).

In the work of He et al. (He et al., 2009), an Adaboost-cascade iris detector is built to extract a rough position of the iris centre and then the centre and radius of the circular iris are localised by employing an elastic model named "*pulling and pushing*". The segmentation of the pupil and iris by fitting a rotated ellipse, after a sequence of procedures for compensating the detected noise, was proposed by Zuo and Schmid (Zuo and Schmid, 2010).

Since iris boundaries are often not circular or elliptical, curve fitting techniques can be valuable to approximate real iris contours (Proença et al., 2010). To further improve segmentation performance, recent methods attempted to use active contour models to accurately localise irregular iris boundaries (Daugman, 2007; Vatsa et al., 2008; Shah and Ross, 2009). The approach taken by Chen et al. (Chen et al., 2010) consisted in detecting the sclera region of the eye, thresholding and filtering the image to detect a rectangular region for iris localization. An edge map of the region of interest is then obtained with a horizontal Sobel operator, and a dynamic programming variation of the CHT algorithm was implemented to detect the limbic boundary. This method corrects the non-circularities of the off-angle iris and combines the intersection of circles obtained by the two CHT algorithms and a linear Hough transform to perform eyelid detection. More recently, Pawar et al. (Pawar et al., 2012) applied geodesic active contours to perform segmentation.

Some works use texture analysis to perform segmentation. Sanchez-Avila et al. (Sanchez-Avila et al., 2002) published a work based on dyadic wavelet transform zero-crossing as iris signature where images were pre-processed by histogram stretching (improving contrast between pupil, iris and sclera) to aid the limbic boundary detection and then, the same algorithm is used inside its area to detect the pupillary

boundary. Nabti and Bouridane's work (Nabti and Bouridane, 2008) is based in a multiscale approach, using Gabor filters and wavelet transform coefficients, to improve edge detection process that determines the success of iris segmentation.

Gradient vector field based methods have appeared in literature such as in the work of Chen et al. (Chen et al., 2011). In this work gradient flow around the iris center plays an important role in the segmentation of the limbic contour.

When analysing most of the methods cited in the literature, it is possible to detect some main drawbacks. In almost all of these methods, inner and outer boundaries, eyelashes and eyelids are detected in different steps, causing a considerable increase in processing time of the system. Usually, the inner and outer boundaries are detected by circle fitting techniques. This is a source of error, since the iris boundaries are not exactly circles and in noisy situations, the outer boundary of iris may not present sharp edges. In some of the aforementioned algorithms, there are a lot of implicit or explicit assumptions about the acquisition process, which are no longer valid in unconstrained acquisition scenarios. Therefore, some of the promising results reported in the literature must be taken with caution and reassessed under these new, more challenging, conditions.

In recent years it has been recognized that the path forward, regarding iris recognition, is the development of algorithms that can work independently of subject collaboration and proper NIR illumination conditions, in order to achieve robust (i.e. accurate even with noisy images) and unconstrained (i.e. accurate for several sets of acquisition conditions: distance, movement, illumination) iris recognition and, in this way, become a real-world applicable method (Ross, 2010). This paradigm shift led to the rise of new trends in the research of iris recognition, for example, exploring VL illumination instead of NIR.

3 SIMULTANEOUS DETECTION OF IRIS CENTRE AND LIMBIC CONTOUR

Researchers are now paying more attention to the context to aid visual recognition processes. Context plays an important role in recognition by the human visual system, with many important visual recognition tasks critically relying on it.

The proposed work aimed to accomplish accurate iris segmentation by using simultaneously acquired

information from two main sources: *iris centre* and *limbic contour*. Both sources contribute to discriminate between a series of iris segmentation candidates. Context information regarding typical iris characteristics in eye images, namely colour and shape, represented the basis of the developed algorithm. By using more than a single source of information, we aimed to lower the misdetection of areas likely to be wrongly segmented, such as eyebrows and glass frames.

3.1 Algorithm Overview

The main steps of the proposed algorithm are systematised in Figure 1. A simplification is adopted in relation to the main rationale outlined above. The simultaneous detection of the iris centre and limbic contour will be addressed by first over-detecting centre candidates, followed by a contour detection around each of them.

The centre candidates are estimated by a method resembling the use of convergence index filters (Kobatake and Hashimoto, 1999). Next, a window centred in each candidate is converted into the polar domain and a shortest path algorithm is used to determine good closed paths around the centre. Using combined data from the centre and respective contour, the best pair centre/contour is selected.

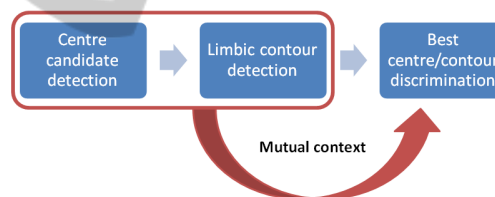


Figure 1: Flowchart of the proposed iris segmentation algorithm.

Typical iris images present two very distinct regions: a high intensity region corresponding to the eye and the skin, and the iris region, at least *partially circular* and *lower in intensity*. These two sources of knowledge can be presented separately but are intrinsically connected. The fact that the iris is a darker region against a brighter background translates into a specific divergent gradient orientation from its centre. At the same time the limbic contour (iris outer edge) will present a high gradient magnitude as well as a closed shape. The approach taken in this work was that of detecting pairs of iris centre and limbic contour candidates that maximise a quality factor weighted by the aforementioned combined knowledge.

3.2 Iris Centre Detection

Iris centre candidates are detected using a template

matching algorithm based on gradient vector field orientation. Theoretically the gradient is a vector field that points in the direction of the greatest rate of increase of a scalar field. Considering an image as a scalar field, it is easy to perceive the gradient as a vector field that points from darker regions (of lower intensity) towards brighter regions (of higher intensity). Figure 2(b) depicts a simple example of gradient vector field orientation on a synthetic image. The expected behaviour of vectorial divergence from darker regions to brighter regions is observed. These observations can be easily extrapolated to typical eye images.

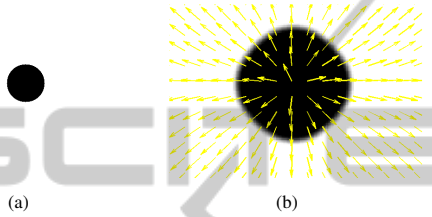


Figure 2: Gradient orientation vector field in synthetic images. Notice how the vector field diverges from darker regions and converges to brighter regions.

The iris is surrounded by two distinct higher intensity regions: the sclera and the skin. With this in mind a divergent gradient orientation is expected from the center of the iris towards the aforementioned brighter regions, as observed in Figure 3(b).

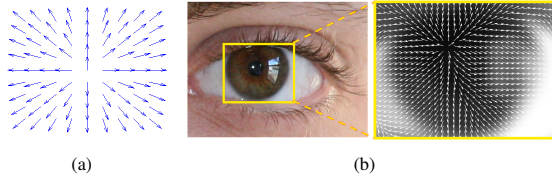


Figure 3: The iris centre detection is based on two vector fields: a) Template vector field and b) Gradient orientation vector field.

The centre candidates are, thus, detected by computing the cross-correlation, c_{corr} , between the gradient vector field orientation and the divergent template vector field depicted in Figure 3(a). The c_{corr} values are calculated as:

$$c_{corr} = (f * g)[\mathbf{n}] \stackrel{def}{=} \sum_{\mathbf{m}} f^*[\mathbf{m}]g[\mathbf{n} + \mathbf{m}] \quad (1)$$

where f and g represent the gradient orientation vector field and the template vector field respectively. The resulting c_{corr} matrix can be graphically represented as exemplified in Figure 4(a), where the values range from -1 to 1 , with -1 being represented in blue

and 1 in red. The centre candidates are detected as the N local maxima with the highest c_{corr} values.

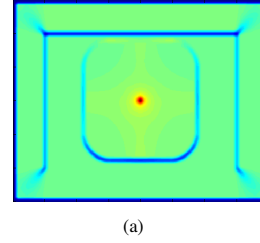


Figure 4: Cross-correlation results on the synthetic image from Figure 2(a).

3.3 Limbic Contour Detection

In the proposed method for limbic boundary detection we consider the image grid as a graph, with pixels as nodes and edges connecting neighbouring pixels. With this in mind the proposed algorithm defines a limbic contour candidate as the best closed contour around a given centre candidate.

The computation of this best contour is simplified by working in polar coordinates (relative to each iris centre candidate). In this domain a closed contour around a given point becomes a curve from the left side of the polar image ($\theta = 0^\circ$) to the right side of the same image ($\theta = 360^\circ$). With the aforementioned consideration of the image as a graph, computation of the best closed contour becomes computation of the shortest left-to-right path in polar domain. To better understand the proposed limbic contour detection algorithm, we start by introducing some graph concepts (Oliveira et al., 2012).

3.3.1 Graph Concepts

A graph $G = (V, A)$ is composed of two sets V and A . V is the set of nodes, and A the set of arcs (p, q) , $p, q \in V$. The graph is *weighted* if a weight $w(p, q)$ is associated to each arc. The weight of each arc, $w(p, q)$, is a function of pixels values and pixels relative positions. A path from vertex (pixel) v_1 to vertex (pixel) v_n is a list of unique vertices v_1, v_2, \dots, v_n , with v_i and v_{i+1} corresponding to neighbour pixels. The total cost of a path is the sum of each arc weight in the path $\sum_{i=2}^n w(v_{i-1}, v_i)$.

A path from a source vertex v to a target vertex u is said to be the *shortest path* if its total cost is minimum among all v -to- u paths. The distance between a source vertex v and a target vertex u on a graph, $d(v, u)$, is the total cost of the shortest path between v and u .

A path from a source vertex v to a sub-graph Ω is said to be the shortest path between v and Ω if its total

cost is minimum among all v -to- $u \in \Omega$ paths. The distance from a node v to a sub-graph Ω , $d(v, \Omega)$, is the total cost of the shortest path between v and Ω :

$$d(v, \Omega) = \min_{u \in \Omega} d(v, u). \quad (2)$$

A path from a sub-graph Ω_1 to a sub-graph Ω_2 is said to be the shortest path between Ω_1 and Ω_2 if its total cost is minimum among all $v \in \Omega_1$ -to- $u \in \Omega_2$ paths. The distance from a sub-graph Ω_1 to a sub-graph Ω_2 , $d(\Omega_1, \Omega_2)$, is the total cost of the shortest path between Ω_1 and Ω_2 :

$$d(\Omega_1, \Omega_2) = \min_{v \in \Omega_1, u \in \Omega_2} d(v, u). \quad (3)$$

3.3.2 Algorithm for Limbic Contour Detection

Intuitively, the limbic boundary appears as a closed contour in the image, enclosing the iris centre, and over pixels with a strong transition in the grey-level values. Assuming that paths through pixels with high gradient are preferred over paths through low gradient pixels, the limbic contour can then be found among the shortest closed paths enclosing the iris centre candidate.

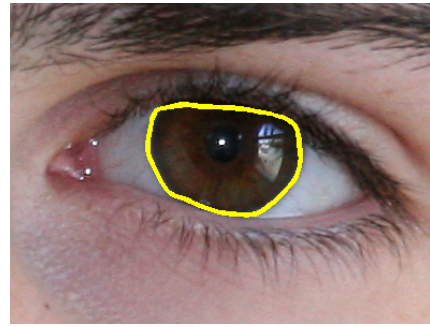
A difficulty with searching for the shortest closed path enclosing a given point C is that small paths, collapsing in the point C , are naturally favoured. We overcome that difficulty by working on polar coordinates. We assume that the origin of the coordinates is the candidate iris centre.

A circular window centred in each candidate is transformed to polar coordinates. A closed path in the original Cartesian coordinates (Figure 5(a)) is transformed into a path from left to right margins in the window in polar coordinates, starting and ending in the same row of the transformed window (Figure 5(b)).

Note that the main assumptions are a) the candidate centre lies within the true limbic contour; b) the limbic contour constitutes a closed path over pixels of strong gradient. The limbic contour is not necessarily circular and the candidate centre does not need to match the true iris centre for a correct contour detection. As long as one centre candidate lies within the iris region one closed contour around it will be detected, regardless of the distance between the detected iris centre candidate and the real iris centre.

3.3.3 Computation of the Shortest Closed Path

In spite of the efficiency of the computation of the shortest path between the whole left and right margins, or between two pre-defined points in the margins, or between one of the margins and a pre-defined



(a)



(b)

Figure 5: a) Original limbic contour in Cartesian coordinates; b) corresponding left-to-right path in the polar domain.

point in the other margin, the search for the shortest path between the left and right margins with the constraint that the path should start and end in the same row seems to increase the complexity of the procedure. As typical, optimization with constraints is more difficult than without.

Had one been interested in the simple shortest path between the left and right margin and the computation would be very efficiently performed using dynamic programming. Assuming the simplifying assumption that the vertical paths do not zigzag back and forth, up and down, in the transformed image, the search may be restricted among connected paths containing one, and only one, pixel in each column between the two end-columns.

Formally, let I be an $N_1 \times N_2$ window (after polar coordinate transform) with N_1 columns and N_2 rows; define an admissible path to be

$$s = \{(x, y(x))\}_{x=1}^{N_1}, \text{ s.t. } \forall x |y(x) - y(x-1)| \leq 1,$$

where y is a mapping $y: [1, \dots, N_1] \rightarrow [1, \dots, N_2]$. That is, an admissible path is an 8-connected path of pixels in the image from left to right, containing one, and only one, pixel in each column of the image.

The first step is to traverse the image from the second column to the last column and compute the cumulative minimum cost C for each entry (i, j) :

$$C(i, j) = \min \begin{cases} C(i-1, j-1) + w(p_{i-1, j-1}; p_{i, j}) \\ C(i-1, j) + w(p_{i-1, j}; p_{i, j}) \\ C(i-1, j+1) + w(p_{i-1, j+1}; p_{i, j}) \end{cases},$$

where $w(p_{i, j}; p_{l, m})$ represents the weight of the edge incident with pixels at positions (i, j) and (l, m) . At the end of this process,

$$\min_{j \in \{1, \dots, N_2\}} C(N_1, j)$$

indicates the end of the minimal connected path. Hence, in the second step, one backtrack from this minimum entry on C to find the optimal path.

Note that this procedure gives not only the shortest path between the left and right margins but also yields the shortest path between any point in the right margin and the whole left margin: for any point (N_1, j) in the right margin, $C(N_1, j)$ indicates the cost of the shortest path between (N_1, j) and the whole left margin, see Figure 6. Finally, it should be clear how to change the initial conditions of the above procedure to yield the shortest path between two pre-defined points in the opposite margins.

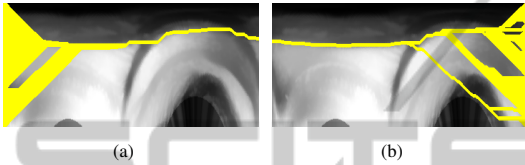


Figure 6: Example of shortest path starting point detection. (a) shows all paths from the left margin to the right margin and (b) all the paths from the right margin to the left margin. As is easily deductable, at least one closed contour will result from this process.

Unfortunately, the computation of the shortest path constrained to start and end in the same row (corresponding to closed contours in the original window) does not seem amenable to such an efficient procedure. The brute force solution of computing the shortest path between the i -point in the left margin and the i -point in the right margin, for $i = 1 \dots N_2$, and taking the minimum, is not compatible with requirements of near real-time in our application.

Noting that if j and ℓ are two distinct points in the right margin, then the shortest paths between each of these points and the whole left margin do not intersect, it is trivial to conclude that there is at least one point m in the right margin for which the shortest path between m and the whole left margin starts also at row m . Note that the paths correspond to closed paths in the original window in Cartesian coordinates (not necessarily including the shortest one). Similarly, interchanging the role of the left and right margin, it is possible to obtain at least one point n in the left margin for which the shortest path to the whole right margin is closed. By computing all the paths from the left to the right margin (and vice-versa), a set of k closed contours is obtained for each centre candidate. The procedure is illustrated in Figure 6.

3.3.4 Design of the Weight Function

The weight of an edge in the graph is a function of the values of the incident nodes (pixels). We start by computing the derivative in the radial direction (centred in

the iris candidate position) in the original space, using a 3-point numerical differentiation, as defined in Eq. (4).

$$G_\theta(r) = \frac{I(r+h) - I(r-h)}{2h} \quad (4)$$

In the graph, to each edge incident with 4-neighbouring pixels correspond a weight determined by the derivative value of the two incident pixels, expressed as an exponential law, presented in Eq. (5).

$$f(g) = f_\ell + (f_h - f_\ell) \frac{\exp(\beta(255 - g)) - 1}{\exp(\beta 255) - 1} \quad (5)$$

with $f_\ell = 2$, $f_h = 32$, $\beta = 0.0208$ and g is the minimum of the derivative computed on the two incident pixels. For 8-neighbour pixels the weight was set to $\sqrt{2}$ times that value. The parameter β was experimentally tuned using a grid search method. The remaining parameters were manually optimised in some of our previous works (Oliveira et al., 2012).

3.4 Best Pair Centre/Contour

From the previously described steps a set of centre/contour candidate pairs (Cp) is built. An example of such candidate pairs is depicted in Figure 7, where the yellow circles represent the centres and the purple curves the limbic contour candidates.

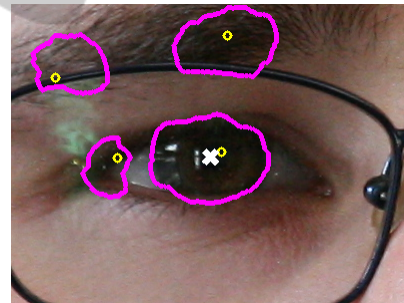


Figure 7: Example of the centre/contour set of candidates. The centre candidates are represented by yellow circles, the detected contours by purple curves and the ground-truth iris centre by a white cross.

The joint decision for the centre and contour is taken to maximise the joint probability of the individual parts. In here, we assume that the joint probability is a monotonous function of the product of individual measures of quality, combined in an overall quality factor, Q . The discrimination between candidates is performed by choosing the pair with the highest Q . The quality factor is given by:

$$Q(Cp) = \frac{\mu(\Delta C) \cdot \rho_p}{|1 - S(C)|} \quad (6)$$

where $\mu(\Delta C)$ is the mean derivative alongside the contour, ρ_p is the cross-correlation value of the centre

candidate, and S is the shape factor of the contour (with perimeter P and area A), given by:

$$S(C) = \frac{4\pi \cdot A}{P^2} \quad (7)$$

This way the best centre/contour pair, Cp_Q , is selected based on mutual information from both iris centre and limbic contour quality.

3.5 Upper Eyelid Approximation

Eyelids represent one of the most common noise factors on images acquired under unconstrained settings when compared with images acquired in controlled environments. Even though the proposed algorithm presents no shape constraints, dark regions, such as eyelashes and shadows, generally pose difficulties to the shortest path algorithm. To encompass such difficulties a simple eyelid approximation algorithm is proposed, based, once again on graph notions. The algorithm is very similar to the one proposed for limbic contour segmentation. It presents two main differences:

- The shortest left-to-right path is computed on the original image in Cartesian coordinates;
- No cost function is designed, and the cost associated with each edge is now given by the minimum intensity of each incident pixel.

With such premises the left-to-right shortest path algorithm, applied to the original iris image, will preferentially stick to low intensity left-to-right curves. As the eyelashes often accumulate on the upper eyelid, creating a low intensity region over the iris, the shortest path will tend to traverse such region.

The lower eyelid was not detected as the eyelashes tend to be longer and considerably more dense in the upper eyelid, than in the lower eyelid. The observed contrast between iris and the lower eyelid is, thus, enough so as not to mislead the proposed algorithm. An example of both successful and unsuccessful eyelid localisation is depicted in Figures 8(a) and 8(b) respectively.

4 RESULTS

4.1 Tested Dataset

The proposed algorithm was tested on the UBIRIS.v2 iris image database (Proença et al., 2010). Images in UBIRIS.v2 were captured under non-constrained conditions (at-a-distance, on-the-move and on the visible wavelength), with corresponding realistic noise

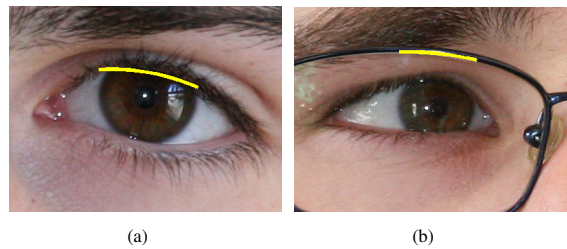


Figure 8: Example of: a) successful eyelid localisation and b) unsuccessful eyelid localisation.

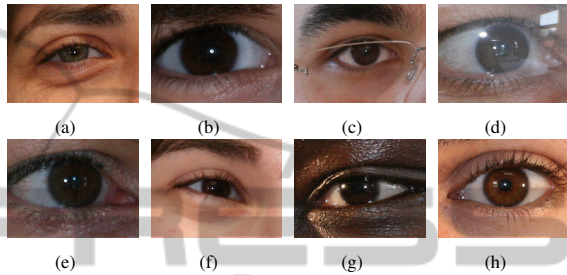


Figure 9: Examples image classes in the UBIRIS.v2 database: a) Heavily occluded; b) Heavily pigmented; c) Glasses occlusion; d) Reflection occlusion; e) Off-angle; f) Rotated eye; g) Black subjects and h) Normal.

factors. Figure 9 depicts some examples of these noise factors (reflections, occlusions, pigmentation, etc.). A subset of the original database, composed by 802 images from 36 distinct individuals was created. All images and individuals were randomly selected, so as to better encompass the widest possible range of noise factors. All images from the created subset were manually annotated for the limbic and pupillary contour, as well as for the geometric center of the iris region.

4.2 Iris Centre Candidate Detection

The accuracy of the centre candidate detection step was analysed by computing the distance between the manually annotated iris centre and each of the N centre candidates. In the proposed work we use $N = 4$ as this value guaranteed that at least one candidate lied inside the iris/pupil region, for every image in the tested dataset. The Euclidean distance between each center candidate and the manually annotated ground-truth centre was computed. The iris centre detection accuracy for a particular image corresponded to the minimum of these distances.

A mean distance of 6.29 ± 5.71 pixels was obtained for the tested dataset. Considering that the mean iris radius of the tested dataset was 58.71 ± 17.45 pixels this result might seem not that promising. The observed deviations of the center candidates

from the real iris center arise mainly from two causes: a) the partial occlusion of the iris by the eyelids results in a deviation from an ideal circular shape and b) the extent to which specular reflections contaminate the iris region causes the gradient flow to diverge towards those regions instead of the sclera.

However, given how the limbic contour detection algorithm is designed, there is no need to achieve perfect accuracy on the real iris centre with any of the detected candidates. As long as one of the candidates lies inside the iris/pupil region, the detection of a closed contour around it (not necessarily centred on it) is guaranteed.

4.3 Best Centre/Contour Pair Discrimination

The discriminative performance of the proposed quality factor, $Q(Cp)$, was analysed by computing the misdetection ratio, M_r . This value corresponds to the ratio between the number of images where the best centre/contour pair was not correctly discriminated and the total number of tested images. To prove that mutual context information improves results obtained by singular sources of information, the M_r values for each $Q(Cp)$ parameter were tested individually:

- The centre/contour pair with maximum ρ_p value
- The centre/contour pair with maximum ΔC value
- The center/contour pair with a $S(C)$ value closest to 1

The M_r values for each individual parameter and for the quality factor are summarized in Table 1. As it can be seen the quality factor overperforms every singular parameter by a considerable margin, presenting a 2.12% value of M_r . Both gradient and cross-correlation based discriminations presented intermediate results, demonstrating limited discriminatory capacity when compared to the mutual context results of the quality factor. Circularity ($|1 - S(C)|$) presents, by far, the worst individual discriminative performance. This observation may lead to one of several conclusions. Either circularity is not a good parameter to be used in the scope of mutual context information, or its effect is only observable when combined to other sources of knowledge. As no attempt was made of testing combinations of two of the three suggested parameters, the true relevance of circularity, as far as discrimination is concerned, cannot be fully asserted.

Table 1: Misdetection ratios observed when the discrimination is performed with each individual parameter and with the proposed quality factor.

Parameter	M_r
ρ_p	0.120
ΔC	0.0860
$ 1 - S(c) $	0.629
Q	0.0212

4.4 Limbic Contour Segmentation Errors

To evaluate the segmentation accuracy of the previously discriminated best limbic contour candidates a series of metrics were computed. All these metrics, listed below, were computed for the initial contour and for the contour after eyelid detection, so as to assert the advantages of this last process. Table 2 summarizes the most relevant results:

- Mean, median and maximum (Hausdorff) distance, in pixels, between the detected limbic contour and the manually annotated ground-truth
- E^1 and E^2 errors, as presented in the NICE.I contest (<http://nice1.di.ubi.pt/>)
- Mean percentage of false iris (FIR) and false non-iris ($FNIR$) segmented pixels

The first three measurements refer to point-to-point distances between the two referred contours. The histogram of errors and the corresponding box plots are depicted in Figures 10(a) and 10(b), respectively.

The information presented in the histogram shows that, besides the percentage of images where the quality factor failed the discrimination of the best centre/contour pair (and thus the largest distances were observed), the segmentation errors are relatively low. The effect of eyelid detection is evident in both results. The histogram of errors after eyelid detection reveals an increased concentration of errors towards lower values. This observation is also supported by the observation of the boxplot results. Lower mean and standard deviation values further corroborate the significant improvement introduced by eyelid detection. The observed influence of the upper eyelid on the segmentation results shows that its detection is a key step of the proposed algorithm. As the eyelashes often present a higher contrast with the skin than the iris with the eyelashes, it is only safe to assume that a gradient weighted shortest path algorithm will tend to prefer the eyelash-skin boundary to the iris-eyelash boundary. Eyelid detection compensates for this fact and results in a significant improvement in all the tested metrics.

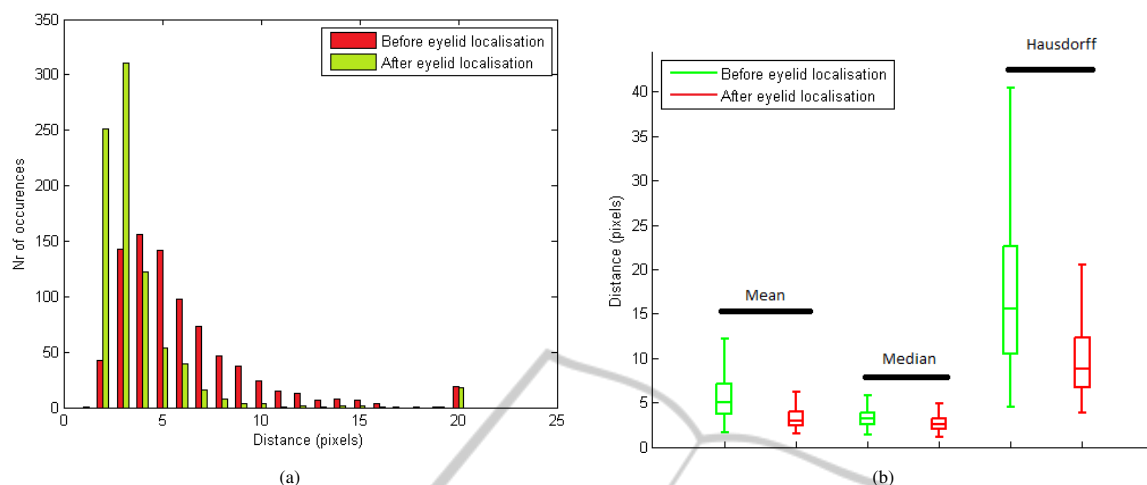


Figure 10: Distribution of the segmentation errors in the tested dataset: a) Histogram of errors (in pixels) and b) boxplots of the error distributions. All the results are presented before and after eyelid detection.

Table 2: Summary of the most relevant segmentation quality measurements before and after eyelid localisation.

	Mean	Median	Hausdorff	E^1	E^2	FIR	$FNIR$
Before eyelid detection	7.11 ± 5.11	4.96	19.47	0.0200	0.0923	0.1814	0.00325
After eyelid detection	4.86 ± 2.96	4.18	12.50	0.109	0.0374	0.0690	0.00583
	Pixels			[0 – 1]			

In 2008 Hugo Proenca and Luis Alexandre, from Universidade of Beira Interior (UBI), Portugal, promoted the NICE.I Contest (<http://nice1.di.ubi.pt/>). This contest aimed to “evaluate the robustness to noise of iris segmentation and noise detection algorithms, toward iris recognition systems within less constrained image capturing conditions, eventually to covert ones, in the near future”. The NICE results represent the great majority of the already available segmentation results using the UBIRISv2 database. However the evaluation parameters of the aforementioned contest are based on two principles that significantly vary from our proposed approach:

1. The segmentation of the iris region of the eye was based both on the detection of the limbic and the pupillary contours. In our work we performed no segmentation of the pupillary contour, as we argue that performing recognition regardless of this step might prove as the path forward, as far as unconstrained iris recognition is concerned. The rationale behind such decision is based on the fact that the contrast between the pupil and the iris is extremely dependent on a set of hardly controlable factors (illumination, iris pigmentation, obstructions, etc.), thus creating a serious challenge as far as the development of robust segmentation algorithms is concerned.
2. The final segmentation results are evaluated as number of pixels correctly classified as iris. This

description takes in consideration the detection of noisy areas (reflections or eyelashes for example) which surpasses the scope of the proposed work.

With these two points in mind it is obvious that a direct comparison with the NICE.I segmentation results is not possible. However the two metrics suggested for the evaluation of iris segmentation in the contest were adapted for the evaluation of the proposed algorithm.

The mean E^1 and E^2 errors for the tested dataset of images are presented in Table 2. The effect of eyelid detection was already ascertained through the analysis of the point-to-point results, but it is of relevance to note that the NICE.I metrics corroborate the previous conclusions.

The obtained E^1 error is lower than all the reported errors in the NICE.I contest (summarized in Table 3). However such a direct comparison will only be possible when noise detection and pupillary estimation are incorporated in the present algorithm. Nevertheless, these preliminary results seem to indicate some promise regarding the chosen approach.

The obtained E^2 value leads to some interesting conclusions. The value presented in Table 3 is the result of a mean FIR of 0.069 and a mean $FNIR$ of 0.0058. A higher FIR value was to be expected as, in most cases, the number of iris pixels in the UBIRIS.v2 images is considerably smaller than the number of non-iris pixels. A 0.0058 $FNIR$ is an excellent in-

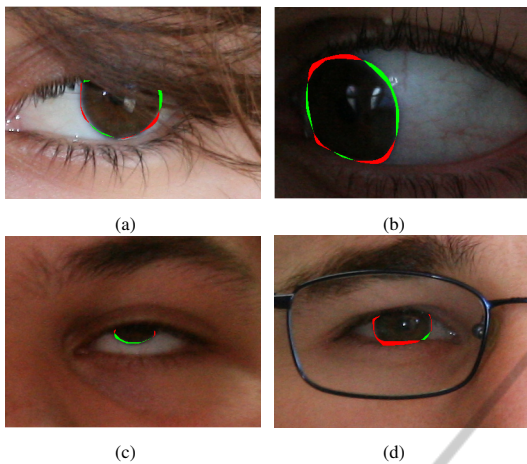


Figure 11: Segmentation examples on images affected by several noise factors. The red points corresponding to the false iris pixels and the green ones to the false non-iris.

Table 3: Comparative analysis between some recent works, including the top performing algorithms in the NICE.I contest, and the proposed methodology.

Author	E^1	E^2
(Tan et al., 2010)	0.0131	–
(Sankowski et al., 2010)	0.0160	0.0600
(Almeida, 2010)	0.0180	–
(Tan and Kumar, 2012)	0.0190	–
Proposed	0.0109	0.0374

indicator that very few iris pixels are classified as non-iris. This means that almost no useful information for recognition is lost during the segmentation process. The mean FIR value, however, indicates a still considerable number of noisy pixels that need to be pruned so as to not present misleading information to the recognition module. Figure 11 depicts some examples of segmentation results in images affected by some of the aforementioned noise factors. One can easily observe that the great majority of the pixels are correctly classified.

5 CONCLUSIONS

The use of mutual information from gradient orientation for centre detection and gradient magnitude for contour detection presented good results for future works. Using the extracted iris regions as inputs for a feature extraction and matching module is the obvious step to carry on after the segmentation algorithm. However some improvements can be easily suggested to the proposed algorithm:

- *Improve Best Centre/Contour Pair Discrimination*: the current discrimination based on the qual-

ity factor is not the most robust measurement. Training classifiers using the ρ_p , $\Delta(C)$ and $S(C)$ values obtained in the tested dataset will generate a far more reliable discrimination module.

- *Noise Detection*: as previously referred the obtained results are only promising to a certain extent. The absence of noise estimation is not acceptable for integration with a recognition module. The number of points that could produce misleading results needs to be significantly reduced in future works.
- *Quality Assessment*: one question that may be posed when working with images acquired under less constrained conditions is if enough information is available so as to allow recognition. A quality assessment module to quantify the amount of textural information, occlusion and focus of individual iris images is an important prerequisite for the application of the proposed algorithm in a functional iris recognition systems.
- *Pupil Probability Estimation*: In this work we did not address the pupil segmentation because of the inherent difficulties presented by the chosen database. We argue that a recognition algorithm with no need of pupillary segmentation is probably the way forwarded in unconstrained acquisition settings. However, the same problem that concerns noise detection is applicable to pupil localisation: if the pixels corresponding to this region are not removed from the segmented iris mask, misleading information will be introduced in the recognition module, resulting in loss of accuracy. As accurate segmentation is rendered difficult by the intrinsic characteristics of the UBIRIS.v2 images, estimating a probability of each pixel belonging to the pupil seems a more robust way of approaching the problem. Future works will certainly focus on these three points of interest.

REFERENCES

- Almeida, P. (2010). A knowledge-based approach to the iris segmentation problem. *Image and Vision Computing*, 28(2):238–245.
- Chen, R., Lin, X., and Ding, T. (2011). Iris segmentation for non-cooperative recognition systems. *Image Processing*, 5(5):448–456.
- Chen, Y., Adjouadi, M., Han, C., Wang, J., Barreto, A., Rishe, N., and Andrian, J. (2010). A highly accurate and computationally efficient approach for unconstrained iris segmentation. *Image and Vision Computing*, 28(2):261–269.

- Daugman, J. (1993). High confidence visual recognition of persons by a test of statistical independence. *IEEE Transactions on Pattern Analysis and Machine Intelligence*, 15(11):1148–1161.
- Daugman, J. (2006). Probing the uniqueness and randomness of iriscodes: Results from 200 billion iris pair comparisons. *Proceedings of the IEEE*, 94(11):1927–1935.
- Daugman, J. (2007). New methods in iris recognition. *IEEE Transactions on Systems, Man, and Cybernetics, Part B: Cybernetics*, 37(5):1167–1175.
- He, Z., Tan, T., Sun, Z., and Qiu, X. (2009). Toward accurate and fast iris segmentation for iris biometrics. *IEEE Transactions on Pattern Analysis and Machine Intelligence*, 31(9):1670–1684.
- Jain, A., Hong, L., and Pankanti, S. (2000). Biometric identification. *Communications of the ACM*, 43(2):90–98.
- Kobatake, H. and Hashimoto, S. (1999). Convergence index filter for vector fields. *IEEE Transactions on Image Processing*, 8(8):1029–1038.
- Ma, L., Tan, T., Wang, Y., and Zhang, D. (2004). Local intensity variation analysis for iris recognition. *Pattern Recognition*, 37(6):1287–1298.
- Masek, L. (2003). *Recognition of Human Iris Patterns for Biometric Identification. Towards Non-cooperative Biometric Iris Recognition*. PhD thesis.
- Nabti, M. and Bouridane, A. (2008). An effective and fast iris recognition system based on a combined multi-scale feature extraction technique. *Pattern Recognition*, 43(3):868–879.
- Oliveira, H., Cardoso, J., Magalhaes, A., and Cardoso, M. (2012). Simultaneous detection of prominent points on breast cancer conservative treatment images. In *Proceedings of the 19th IEEE International Conference on Image Processing*, pages 2841–2844.
- Pawar, M., Lokande, S., and Bapat, V. (2012). Iris segmentation using geodesic active contour for improved texture extraction in recognition. *International Journal of Computer Applications*, 47(16):448–456.
- Proença, H., Filipe, S., Santos, R., Oliveira, J., and Alexandre, L. A. (2010). The ubiris.v2: A database of visible wavelength iris images captured on-the-move and at-a-distance. *IEEE Transactions on Pattern Analysis and Machine Intelligence*, 32(8):1529–1535.
- Radman, A., Jumari, K., and Zainal, N. (2012). Iris segmentation in visible wavelength environment. *Procedia Engineering*, 41:743–748.
- Ross, A. (2010). Iris recognition: The path forward. *Computer*, 43(2):30–35.
- Sanchez-Avila, C., Sanchez-Reillo, R., and de Martin-Roche, D. (2002). Iris-based biometric recognition using dyadic wavelet transform. *Aerospace and Electronic Systems Magazine, IEEE*, 17(10):3–6.
- Sankowski, W., Grabowski, K., Napieralska, M., Zubert, M., and Napieralski, A. (2010). Reliable algorithm for iris segmentation in eye image. *Image and Vision Computing*, 28(2):231–237.
- Shah, S. and Ross, A. (2009). Iris segmentation using geodesic active contours. *IEEE Transactions on Information Forensics and Security*, 4(4):824–836.
- Tan, C. and Kumar, A. (2012). Unified framework for automated iris segmentation using distantly acquired face images. *IEEE Transactions on Image Processing*, 21(9):4068–4079.
- Tan, T., He, Z., and Sun, Z. (2010). Efficient and robust segmentation of noisy iris images for non-cooperative iris recognition. *Image and Vision Computing*, 28(2):223–230.
- Vatsa, M., Singh, R., and Noore, A. (2008). Improving iris recognition performance using segmentation, quality enhancement, match score fusion, and indexing. *IEEE Transactions on Systems, Man, and Cybernetics, Part B: Cybernetics*, 38(4):1021–1035.
- Wildes, R. (1997). Iris recognition: an emerging biometric technology. *Proceedings of the IEEE*, 85(9):1348–1363.
- Zuo, J. and Schmid, N. (2010). On a methodology for robust segmentation of nonideal iris images. *IEEE Transactions on Systems, Man, and Cybernetics, Part B: Cybernetics*, 40(3):703–718.